

Dielectrophoretic characterization of cells in a stationary nanoliter droplet array with generated chemical gradients

Tom Ben-Arye^{1,2} · Sinwook Park³ · Jonathan Shemesh⁴ · Dan Peer⁵ · Shulamit Levenberg^{1,2} · Gilad Yossifon³

Published online: 19 August 2015
© Springer Science+Business Media New York 2015

Abstract A novel design of reusable microfluidic platform that generates a stationary nanoliter droplet array (SNDA) for cell incubation and analysis, equipped with a complementary array of individually addressable electrodes for each microwell is studied. Various solute concentration gradients were generated between the wells where dielectrophoresis (DEP) was used to characterize the effect of the gradients on the cell's response. The feasibility of generating concentration gradients and observation of DEP responses was demonstrated using a gradient of salts in combination with microparticles and viable cells. L1210 Lymphoma cells were used as the model cells in these experiments. Lymphoma cells' cross-over frequency (COF) decreased with increasing stress conditions. Specifically, a linear decrease in the cell COF was

measured as a function of solution tonicity and blebbistatin dose. Lymphoma cells were incubated under a gradient of the chemotherapeutic agent doxorubicin (DOX), which led to saturation in the cell-COF response at 30 nM DOX, demonstrating the potential of the platform in screening of label-free drugs.

Keywords Microfluidics · Cell analysis · Dielectrophoresis

1 Introduction

Microfluidic systems have been proven an efficient tool for studying cell biology, enabling the precise control of the cell microenvironment and the integration of various microfluidic tools, such as chemotherapy, high-throughput screening and electroporation (Velve-Casquillas et al. 2010; El-Ali et al. 2006; Gao et al. 2012; Geng and Lu 2013; Park et al. 2014; Avesar et al. 2014). Microfluidic gradient generators offer high precision and control over spatiotemporal gradients as compared to traditional methods, and can be used to understand cues in biological processes such as chemotaxis, morphogenesis and cancer metastasis (Kim et al. 2010; Wang et al. 2004; Vickerman et al. 2008). Variety of gradient-generating approaches have been developed, driven either by the diffusion and the convection of laminar flow (Jeon et al. 2000; Yang et al. 2011; Ismagilov et al. 2000) or by free-diffusion along a channel (Kim et al. 2009; Abhyankar et al. 2006; Du et al. 2009; Mosadegh et al. 2007). The former provides excellent control over gradient stability, profile and concentration range, but is unsuitable for cell incubation and analysis, due to the loss of most of the secreted signaling factors or the wash of non-adherent cells. The latter produces chemical gradients with stagnant fluidic condition, but it is difficult to maintain a stable gradient profile over time. To

T. Ben-Arye and S. Park contributed equally to this work.

Electronic supplementary material The online version of this article (doi:10.1007/s10544-015-9996-z) contains supplementary material, which is available to authorized users.

✉ Gilad Yossifon
yossifon@technion.ac.il

- ¹ Department of Biomedical Engineering, Technion, 32000 Haifa, Israel
- ² Russell Berrie Nanotechnology Institute, Technion, 32000 Haifa, Israel
- ³ Faculty of Mechanical Engineering, Micro- and Nanofluidics Laboratory, Technion, 32000 Haifa, Israel
- ⁴ Department of Mechanical and Manufacturing Engineering, UNSW Australia, Sydney, NSW, Australia
- ⁵ Laboratory of NanoMedicine, Department of Cell Research and Immunology, Department of Material Science and Engineering, and the Center for Nanoscience and Nanotechnology, Tel Aviv University, 69978 Tel Aviv, Israel

overcome these limits, some groups have developed microfluidic gradient generators with integrated microvalves, (Frevert et al. 2006) storage microwell arrays, (Selimović et al. 2011) 3D-structures using hydrogels, (Vickerman et al. 2008; Liu et al. 2009) and encapsulation of cells in droplet arrays (Sun et al. 2011). But there are still vast challenges, demanding microfluidic platforms which can integrate precise control of gradient formation, cell microenvironments, long-term incubation and a large scale high throughput array for simultaneous screening.

Typically, cellular behaviors triggered by chemical gradients can be analyzed by either observation of cell migration (Wang et al. 2004; Vickerman et al. 2008; Liu et al. 2009; Nie et al. 2007) or cell fate (e.g., proliferation and differentiation of neural stem cells (Chung et al. 2005)) in micro-scale systems. However, these methods are difficult to precisely quantify cell behaviors on gradients with high resolution. Even though the developed platforms can produce stable and controllable gradients over the cells, analysis of the cell response (e.g., cell migration, cell viability assays) is limited by poor outcome resolution. Therefore, novel cell characterization platforms, enabling precise quantification need to be developed, particularly for non-adherent cell types.

The stationary nanodroplet array (SNDA) is a polydimethylsiloxane (PDMS)-based microfluidic platform, suitable for incubation and analysis of adherent and non-adherent single cells (Shemesh et al. 2014). The system generates an array of stationary nanodroplets, on a surface of choice, via microwells that branch off of a main microfluidic channel. The uniqueness of this platform lies in a system of secondary vents, called restrictions, which allow air to escape the system during the loading step (Movie S1). This feature allows the user to choose the surface which is in contact with the cells and supports work under low pressures, eliminating the need for permanent sealing of the PDMS platform to the surface, rendering the system reusable. In addition, after the device is loaded with cells, a chemical gradient can be formed between the wells, which can be used for high resolution assessment of the effect of various concentrations of a solute on cell response. This system requires minute amounts of reagents and cells, and is useful for studying rare species of cells.

Dielectrophoresis (DEP) is defined as the translational motion of neutral particles due to effects of polarization in a non-uniform electric field (Pohl and Pohl 1978). DEP is an established technique that is used for probing and/or manipulating cells and bio-particles, in which the unique dielectric properties of cells are analyzed using alternating current (AC) fields (Gagnon 2011; Voldman 2006; Khoshmanesh et al. 2011). In particular, a crossover frequency (COF), which is an AC frequency at which the DEP vanish, i.e. cells shift from attraction (positive DEP) to repulsion (negative DEP), can be used as a sensitive discriminator between different cell types or cell conditions and can be utilized for cell separation and

characterization. We have recently employed this method for characterization of cells under continuous flow conditions (Rozitsky et al. 2013).

Here, we combined the PDMS-based microfluidic platform and the DEP COF technique into a generic lab-on-a-chip platform that enables the generation of both an array of nanoliter droplets and a chemical gradient, alongside the capacity to perform DEP characterization of individual microwells, via an embedded electrode array. Beads or non-adherent lymphoma cell in a gradient of KCl or phosphate buffered saline (PBS), respectively, were used as a model system to assess the performance of the chemical gradient formation. An osmotic pressure gradient was formed to study the effect of tonicity on cell DEP. Blebbistatin and doxorubicin (DOX), representing a molecular inhibitor and a cytotoxic drug, respectively, were used to demonstrate gradient effects at the cellular level.

2 Material and methods

2.1 Chip design and fabrication

The SNDA-DEP platform was generated by aligning the microfluidics PDMS-based microwell array, with a substrate which contained a complementary electrode array (Fig. 1). The PDMS-based SNDA consists of an array of two rows of one hundred wells of 8 nanoliter volume, branching from a main microfluidic channel (width 300 μm and length 41 mm) with secondary air evacuation vents (side channel width 100 μm) connected to the wells through narrow restrictions (see also Fig. S1 in the supporting materials). It is suitable for single- or multi-cell incubation and analysis, with a gradient of chemical composition in isolated environments separated by immiscible fluorocarbon oil (Fluorinert FC-40, F9755-100ML, Sigma). The SNDA was fabricated using standard PDMS replica mold techniques, including deep reactive ion etching (DRIE) master fabrication, PDMS molding and water priming for evaporation reduction, as previously described (Shemesh et al. 2014).

The electrode array substrate, which contains various geometries (i.e., hyperbolic quadrupole, rectangular quadrupole and linear) and with varying distances between electrodes (from 50 to 150 μm), was fabricated using photolithography and wet-etching processes (Fig. S2). Layers of Au/Cr (30 nm/200 nm in thickness) were evaporated on a 4-in. Pyrex glass wafer. Then, standard photolithography was performed to create the electrode pattern. The exposed Au/Cr surface was wet-etched. After the SNDA and the electrode array were fabricated, they were manually aligned, using a Nikon TI inverted microscope, to form a hermetic, yet reversible seal.

Although we can potentially measure the DEP of the entire array at single-well resolution, for simplicity purposes, the

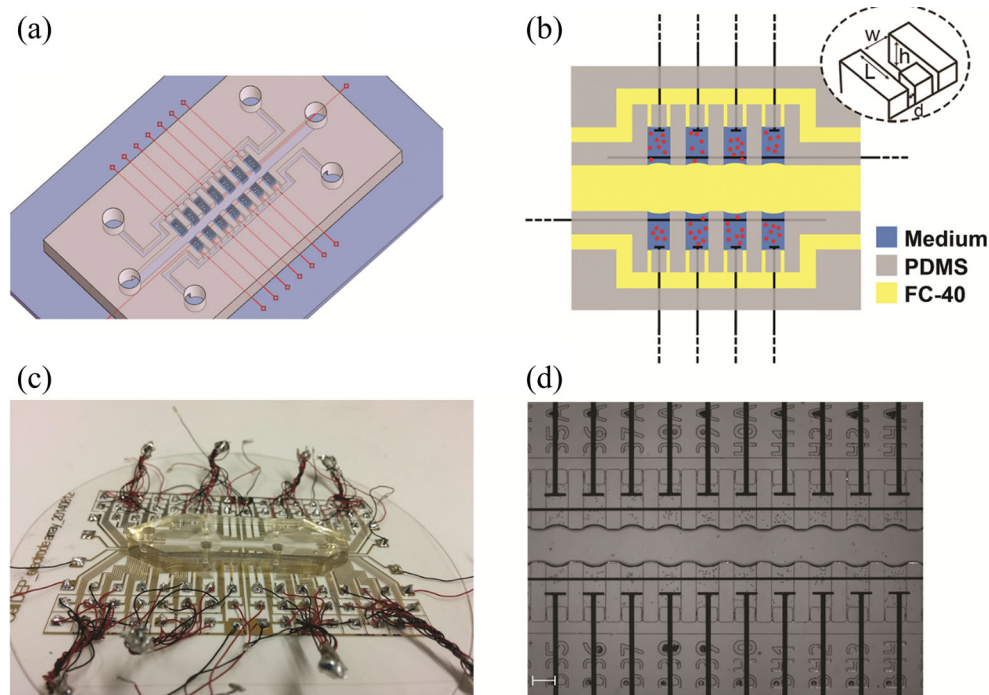


Fig. 1 The SNDA-DEP device structure. **a** Three-dimensional schematic depiction of the SNDA-DEP device; **b** Two-dimensional illustration of a solute gradient over cells (red) within microwells (white-blue) situated inside the PDMS walls of the SNDA (grey), separated by fluorocarbon oil (yellow), each with an individually addressable electrode (black). Inset

depicts the dimensions of the well where $d = 2 \mu\text{m}$, $h = 100 \mu\text{m}$, $w = 200 \mu\text{m}$ and $L = 400 \mu\text{m}$; For clarity purposes the number of wells depicted in the schematics is much smaller than in the actual chip; **c** Photograph of the SNDA-DEP device; **d** Bright-field image of the wells isolated by immiscible oil FC-40. Scale bar $200 \mu\text{m}$

electrodes of every ~ 13 microwells (16 groups) were shared with one wire connection. The electrode array was designed to characterize the per-well DEP or electrorotation response arising from biological changes, such as dimension, shape, conductivity and permittivity of the cell or changes in the surrounding electrolyte concentrations (Morganti and Morgan 2011).

2.2 Cell preparation and reagents

Non-adherent mouse lymphoma cells (L1210) were cultured in cell medium comprised of Dulbecco's Modified Eagle medium (Gibco), 10 % FBS (HyClone), 1 % Pen-Strep (Biological Industries), 1 % GlutaMAX (Life Technologies), and 1 % sodium pyruvate (Life Technologies). In the short term experiments (tonicity and salt gradient experiments), cells were washed three times in the measurement buffer and loaded into the device, at an average cell density of 10 cells per well. Cells were washed by centrifugation (500 g, 5 min), followed by aspiration of the supernatant and resuspension of the cells in the measurement buffer. In the long-term experiment (DOX and blebbistatin gradient experiments), cells, suspended in cell medium supplemented with an additional 10 % FBS, were loaded into the SNDA-DEP device 24 h prior to the DEP measurement, at an average concentration of 2–3 cells per well. Unless stated otherwise, DEP measurement

buffer, which conductivity was $1.445 \pm 0.065 \text{ mS/cm}$, contained 90 % Isotonic Low Conductivity Buffer (ILCB) and 10 % PBS. ILCB includes 8.5 % sucrose (J.T.Baker), 0.3 % D-(+)-glucose (Sigma-Aldrich) and 0.725 % RPMI 1640 medium (Biological Industries).

Since lymphoma cells have a short cell cycle of 12 h (Fig. S3), two cells were seeded per well in the experiments which required 24 h of incubation (Blebbistatin and DOX) inside the SNDA, to reach a final concentration of eight cells per well after the 24-h incubation.

2.3 Generation of chemical gradients and isolated nanoliter droplets

Solute gradients were formed between low (C_{low}) and high (C_{high}) concentration solutions, where the C_{high} solution also contained 0.1 mg/ml fluorescein (Reidel-Dehaen) to quantify the local concentration. The device was first loaded, via the inlet, with cells suspended in a either cell medium or DEP buffer with the C_{low} solution. After the microwells and the main channel of the device were filled, the outlet was filled with the C_{high} solution, creating a unidirectional, slow ($\sim 50 \mu\text{m/s}$) flow driven by hydraulic pressure from the outlet to the inlet. The solute flows by convection in the main channel, and is diluted in the process by diffusion into the microwells. Thus, wells closer to the outlet are exposed to

higher solute concentrations. The gradient formation lasts about 20 min and is tracked using the fluorescein intensity. After the gradient was formed, the droplets in the well-array were isolated by shearing the liquid in the main channel and sheathing the wells with fluorocarbon oil. Then, the C_{low} and C_{high} solutions were loaded to separate bulk reference channels embedded in the device for normalization of the fluorescein intensity. The chemical gradient concentration was then quantified using the fluorescein fluorescent intensity. The C_{high} solution contained, depending on the experiment, either 1 mM KCl (Source) in deionized (D.I.) water, 10 % PBS (Gibco) in ILCB, 8.5 % Sucrose (J.T.Baker) in ILCB + 10 % PBS, 50 μ M blebbistatin (Sigma-Aldrich) in the cell medium or 250 nM DOX (Petrus) in the cell medium. To calculate the solute concentration, the fluorescein intensity was normalized by using the following equation $C_{well} = (C_{high} - C_{low}) \cdot I^* + C_{low} = (C_{high} - C_{low}) \cdot (I_{well} - I_{low}) / (I_{high} - I_{low}) + C_{low}$, where I^* , I_{well} , I_{high} , and I_{low} are the normalized intensity, intensity measured inside the well, intensity of the concentrated solute (0.1 mg/ml fluorescein) reference channel, and the intensity of the low concentration solute (without fluorescein) reference channel, respectively. The detailed procedure for gradient generation and isolation of droplets has been previously reported by Shemesh et al. (2014).

2.4 Medium replacement inside the SNDA

In the experiments involving DOX and blebbistatin, after 24 h of incubation and before the DEP measurement, cell medium was replaced with the measurement buffer ILCB +10 % PBS. In order to replace the medium, the fluorocarbon oil must be removed from the main channel. In this step, oil plugs can form in the entrance of the well, preventing effective medium change. To prevent this, the wells are coated with a hydrophilic protein while the main channel is not. This asymmetric coating is achieved by filling the device with a 1 % bovine serum albumin (BSA, Millipore) solution followed by shearing of the main channel and incubating the device for 30 min, allowing the hydrophilic BSA to coat the PDMS walls of the wells before device alignment.

2.5 Experimental setup for DEP

In order to examine the cell or particle DEP response, 1.25×10^6 nonadherent cells/mL (~ 10 cells/microwell) or 2×10^{-2} v/v% 2 μ m fluorescent polystyrene beads (FluoroMax, Thermo Scientific) were used in all experiments. Cell density was low to prevent cell-to-cell electrical interaction (e.g., cell chain formation) during the DEP measurement, which can cause a bias in the measurement (Gascoyne et al. 2009). Various AC field frequencies with a sinusoidal waveform were applied using a function generator (33250A, Agilent), and the motion of the cells or particles inside the

wells was recorded using an Andor Neo sCMOS camera attached to a Nikon TI inverted epi-fluorescent microscope with a 10 \times objective lens. The COF in each well was obtained by monitoring particle/cell motion either towards (p-DEP) or away from the electrodes (n-DEP). As a comparison, the COF of cells exposed to homogenous reagent concentrations, was measured inside the SNDA-DEP device or using bulk hyperbolic quadrupole 30 μ m-wide microelectrode set at distances of 100 μ m between electrodes, without a microchannel.

2.6 Phalloidin-FITC and DAPI cell staining

Cells were fixed with 2 % paraformaldehyde (PFA, Electron Microscopy Sciences), for 15 min at room temperature, and then permeabilized with 0.3 % Triton X-100 (Bio Lab), for 10 min at room temperature. Phalloidin-FITC (1 μ g/mL; Sigma-Aldrich), for actin filament staining, and 4',6-Diamidino-2-phenylindole (DAPI; Sigma-Aldrich), for nuclear counterstaining, were added for 20 min. The cells were observed under a ZEISS LSM 700 confocal microscope with a 40X water-immersion objective.

2.7 COF-based extrapolation of salt concentrations

In the electrolyte gradient experiments, in addition to the fluorescein intensity, we have used bead or cell measured COF data in determining the KCl or PBS concentrations, respectively. Beads or cells distributed inside the SNDA were exposed to homogenous KCl or PBS concentrations, respectively, were characterized by DEP measurements to be used as a reference (insets of Figs. 2c and 3b). The COF reference curve underwent non-linear fitting for the beads or linear fitting for the cells, enabling translation of COF values to KCl or PBS concentrations.

3 Results and discussion

3.1 Gradient of electrolytes over microbeads

The electrolyte gradient-generating performance of the SNDA was first evaluated by determining changes in particle COF throughout the well array. As a simple target model, a KCl gradient was formed with two solutions, one with 2 μ m fluorescent microbeads in DI water and a second with 1 mM KCl (i.e., measured solution conductivity, $\sigma_m \sim 180$ μ S/cm) and 0.1 mg/ml fluorescein in DI water. A distinct shift in bead COF, from 10 to 700 KHz, and reduced fluorescein intensity were obtained as the well number decreased (Fig. 2a and b and Movie S2), illustrating the effect of the concentration gradient from 1 mM to DI water. Bead COF was measured inside the isolated microwells and correlated to the well number (Fig. 2c). This trend of decreasing COF with increasing

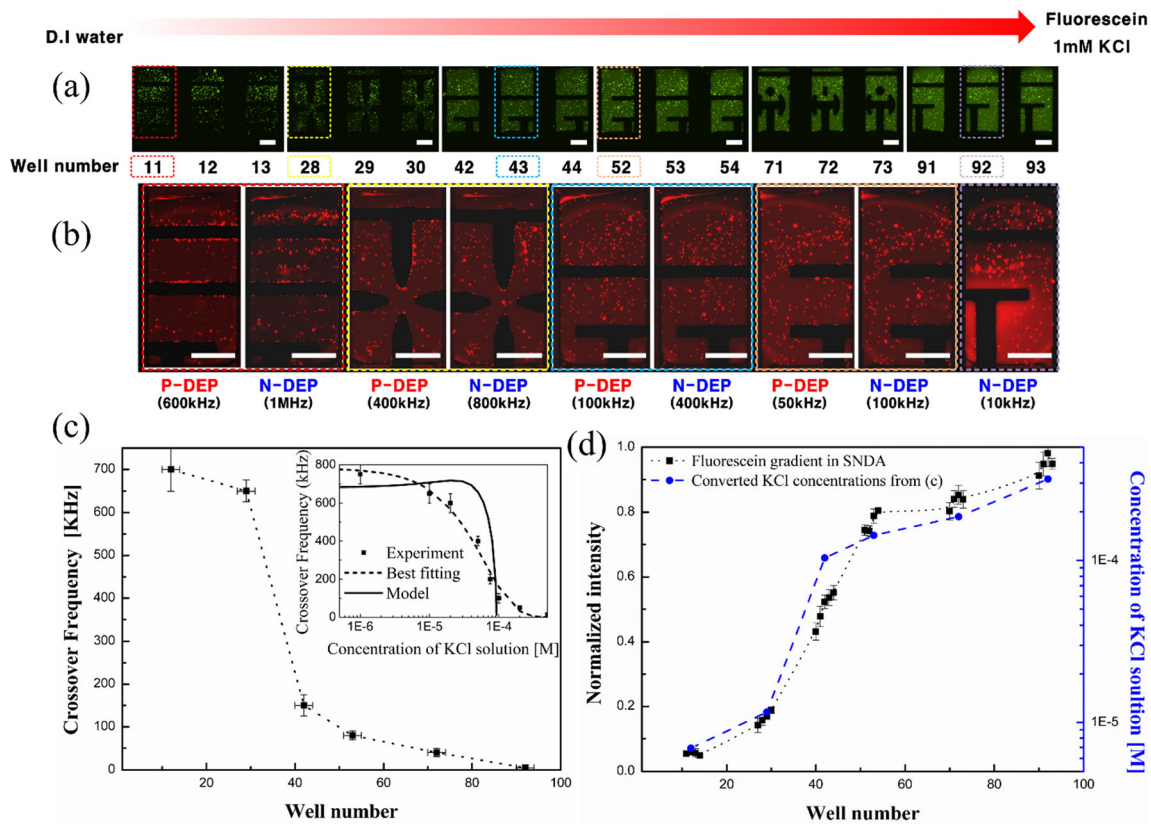


Fig. 2 KCl gradient inside the SNDA and DEP characterization of micro-particles. **a** Images visualizing the fluorescein intensity gradient; **b** Fluorescent images representing attraction (p-DEP) and repulsion (n-DEP) of the 2 μm red particles from the electrodes inside the wells. The COF decreases as the well number increases in correlation with increasing KCl concentrations; **c** COF as a function of the well number inside the SNDA. The inset indicates the best curve fitting (dashed line) of the measured cell COF vs. homogenous KCl concentration (black markers),

which served as a reference for the conversion between COF and KCl concentration. The expression $y=ae^{-bx}$ was used as the fitting equation, where $a = 781.53 \text{ KHz}$, $b = 15,907.08 \text{ M}^{-1}$, $R^2 = 0.966$. The continuous line stands for the fitted COF model Eq. (1); **d** Normalized fluorescein intensity and converted KCl concentration as a function of the well number. The converted KCl concentrations from (c) are depicted as a dashed blue line for comparison with the fluorescein gradient intensity. All scale bars are 100 μm

solution conductivity is in agreement with previous experimental studies (Green et al. 1999; Basuray & Chang 2007). The DEP measurements inside the wells close to the inlet/outlet, below well number 13 or above well number 92, showed COF values close to those measured of cells exposed to homogenous concentrations of the injected solution concentrations (i.e., 1 μM and 1 mM KCl). A steep gradient, of values estimated to range between 10 and 100 μM KCl, developed between wells 30 and 50, as measured both by fluorescein intensity and DEP-COF profiles. This behavior stands in qualitative agreement to the theoretical model for the COF of homogenous spherical particle (Rozitsky et al. 2013).

$$\omega_{COF} = \sqrt{\frac{(\sigma_m - 2K_s/a)(2K_s/a + 2\sigma_m)}{(\epsilon_p - \epsilon_m)(\epsilon_p + 2\epsilon_m)}}, \quad (1)$$

wherein the particle conductivity, $\sigma_p = 2K_s/a$, has been replaced by the more meaningful surface conductance, K_s .

This factor stems from the fact that although polystyrene beads have low intrinsic conductivity, COF measurements indicate the presence of high conductivity which is attributed to a surface conductance component. The fitted surface conductance $K_s = 2.1 \text{ nS}$ is within the range of values obtained in our previous work (Rozitsky et al. 2013). The other parameters are the particle radius $a = 1 \mu\text{m}$, the medium permittivity $\epsilon_m = 80\epsilon_0$, the particle permittivity $\epsilon_p = 4\epsilon_0$, where $\epsilon_0 = 8.85 \cdot 10^{-12} \text{ F/m}$ is the vacuum permittivity. Another fitted parameter was the diffusion coefficient, used for calculating the solution conductivity from the KCl concentration, which is three times larger than that commonly used for KCl ($D = 2 \cdot 10^{-9} \text{ m}^2/\text{s}$). The theoretical model for the COF $f_{COF} = \omega_{COF}/2\pi \text{ Hz}$ is then plotted against the concentration in the inset of Fig. 2c. The converted KCl concentration gradient, based on Fig. 2c, is shown to be in good agreement to that obtained from the Fluorescein intensity (Fig. 2d). Also, a good agreement was observed when comparing the COF response for uniform concentrations either inside the SNDA or bulk experiments using the hyperbolic quadrupole electrode (Fig. S4).

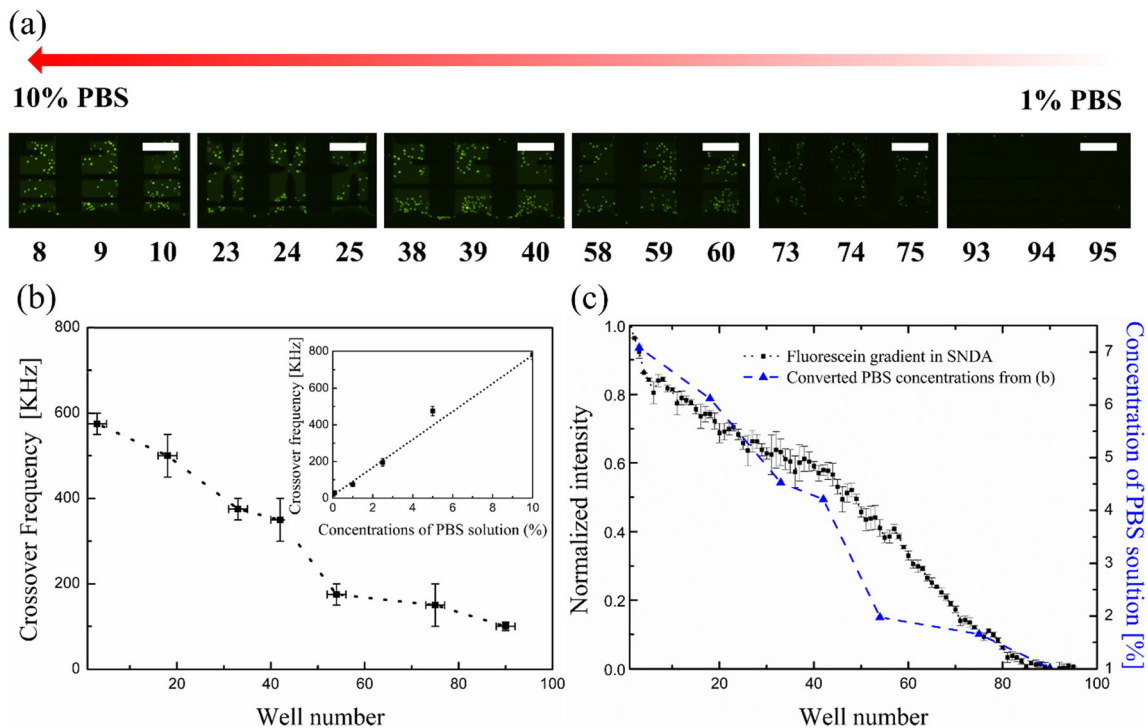


Fig. 3 Cell-DEP characterization under a gradient of PBS. **a** Bright-field and fluorescent microscopy images showing cells inside the microwells with a fluorescein gradient used to visualize the PBS gradient. The *red arrow* indicates the direction of the PBS gradient; **b** Cell COF as function of well number. The inset presents the linear fitting (*black dashed line*) of the measured cell COFs vs. homogenous PBS concentration (*black*

markers), which served as a reference for the conversion between COF and KCl concentration ($R^2 = 0.977$, slope = 76.41 KHz/(% of PBS), intercept = 14.25 KHz); **c** Normalized fluorescence intensity and calculated PBS concentration based on the cell COF, as function of well number. All scale bars are 200 μm

3.2 Gradient of electrolytes over cells

The solution conductivity effect on cell DEP was also characterized inside the SNDA under a gradient of 0.1 % ($\sigma_m = 0.26$ mS/cm) to 10 % ($\sigma_m = 1.51$ mS/cm) PBS in ILCB. The generated gradient was then quantified by both determining the cell COF within the well array and by measuring fluorescein intensity (Fig. 3c). Cell COF as a function of PBS concentration in the bulk hyperbolic quadrupole microelectrode served as a reference. A linear regression model was used to obtain a calibration graph, which was further used to determine the PBS concentration from the COF of the cells (inset of Fig. 3b). The linear relation between the first COF and the solution conductivity is in agreement to the theoretical models (Pethig 2010; Alshareef et al. 2013).

$$f_{COF} = \frac{\sqrt{2}}{2\pi a C_m} \sigma_m, \quad (2)$$

where $C_m = 0.0423 [F/m^2]$ is the fitted capacitance of the cell membrane. While increasing the frequency from 10 KHz to 1 MHz, the cell DEP changed from n-DEP to p-DEP corresponding to the cell's first COF. A second cell COF was not considered here, due the relatively high frequency associated with it, which extends beyond the limit of the equipment

range. PBS concentration decreased with decreasing well number, as did cell-COF, which steadily declined from 580 to 100 KHz, which corresponded to the trend observed in the calibration curve (inset of Fig. 3b) and in agreement with other reported studies wherein a linear relation was predicted (Alshareef et al. 2013; Gascoyne et al. 1997; Ratanachoo et al. 2002). In summary, cell response to chemical gradients can be characterized via the cell-COF inside the SNDA-DEP, and can be correlated with the solute concentration extracted from the fluorescein intensity profile.

3.3 Tonicity gradient

Cells shrivel in hypertonic solutions, resulting in biomolecular changes, (Alshareef et al. 2013) which can affect the cell-COF (Hamdi et al. 2014). To examine the effect of the solution tonicity on the cell-DEP, cells were exposed to a tonicity gradient inside the SNDA-DEP device. A solution tonicity gradient ranging from isotonic (270 mOsm) to hypertonic (520 mOsm) was generated by the non-ionic molecule sucrose (Fig. 4a). After the gradient was formed, cells were further characterized using DEP (Fig. 4a). A linear regression model of the average COF as a function of the solution's tonicity showed a close fit with the actual results ($R^2 = 0.94$)

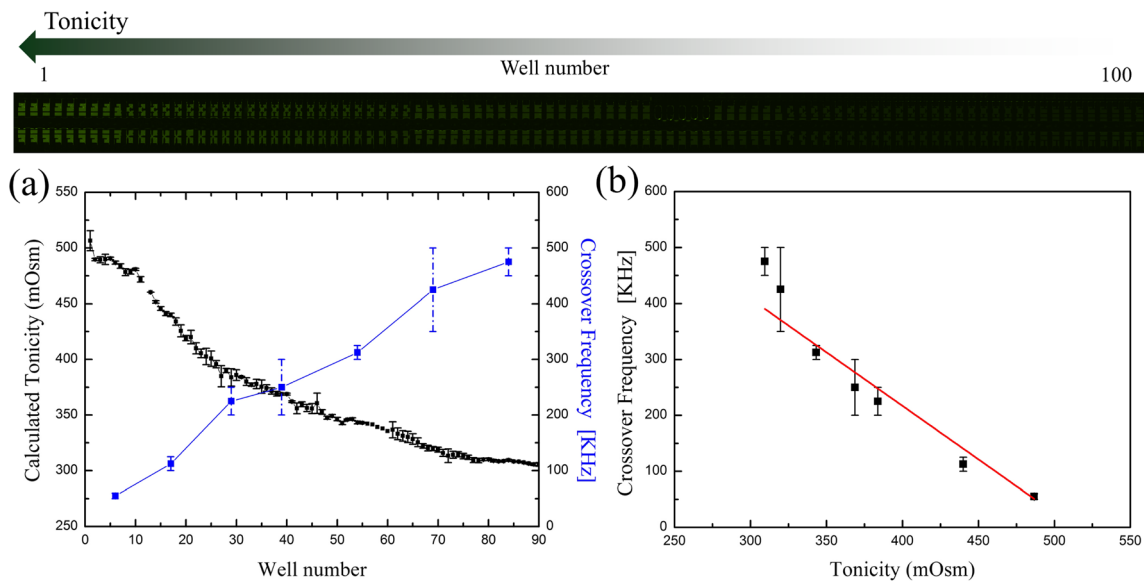


Fig. 4 Cells exposed to a tonicity gradient inside the SNDA-DEP platform. **a** The calculated tonicity and the measured cell-COF as a function of well number; **b** Cell-COF as a function of medium tonicity. The red

dotted line indicates a linear regression of the results. $R^2 = 0.942$, slope = -2.30 KHz/mOsm, intercept = 1140 KHz

(Fig. 4b). The conductivity of the hypertonic and the isotonic solutions was 1.63 ± 0.01 mS/cm and 1.38 ± 0.03 mS/cm, respectively, namely, the hypertonic solution was 18 % more conductive. From our previous observations of the relation between cell-COF and medium conductivity, increasing the medium conductivity is expected to increase cell-COF (Fig. 3). However, although the solution conductivity rose with the tonicity (i.e., lower well number), the cell-COF decreased, suggesting an underlying biological change caused by the solution hypertonicity dominated the cells' COF response. In parallel, we observed a weak change in cell morphology due to the solution's tonicity, resulting in an average 7.8 % decrease in cell diameter between the wells at either end of the gradient (6.1 ± 0.8 μ m in wells 1–5 and 5.6 ± 1.1 μ m wells 85–90) (Fig. S5), amounting to a much more subtle change compared to the COF shift (475 ± 25 KHz to 60 ± 10 KHz). These results demonstrate the capabilities of the SNDA-DEP platform to generate chemical gradients on cells in isolated microenvironments and the characterization of the biological changes the cells undergo with high resolution.

3.4 Blebbistatin gradient effect on cell-DEP

The morphological effect of blebbistatin, an inhibitor of myosin II and F-actin bundle formation, on adherent cells can be easily detected by bright-field microscopy and F-actin staining (Kolega 2004; Duxbury et al. 2004). Cells become round and lose their distinct shape. However this morphological change is not so evident in non-adherent cells, as they are already round. We aimed to use the SNDA-DEP to characterize the effect of blebbistatin concentrations on non-adherent cells. To

this end, a gradient of blebbistatin and fluorescein was generated inside the SNDA containing non-adherent lymphoma cells. After measuring the intensity of the fluorescein inside the wells, cells were incubated for 24 h inside the SNDA 8 nl well array. After the cell medium and the blebbistatin were washed and replaced with the measurement buffer, the cells inside the isolated wells were further characterized using DEP. It was found that cells which were incubated with blebbistatin had a lower COF (Fig. 5a). Using the measured fluorescein signal, the blebbistatin concentration was calculated in each well. A linear regression model of the average COF as a function of the blebbistatin concentration fit the observed results well, with an $R^2 = 0.994$ (Fig. 5b). In addition, the effect of the blebbistatin on the cells was monitored in the bulk. Cells exposed to 10 μ M blebbistatin were larger in diameter, were less densely packed, and contained several nuclei, which could be explained by the difficulty of performing normal cell division under the inhibition caused by the blebbistatin (Fig. 5c).

3.5 DOX gradient

Doxorubicin, an anthracycline antibiotic commonly used in the treatment of hematopoietic and solid tumor, was chosen as a model drug (Cohen et al. 2014; Ganoth et al. 2015). As any cytotoxic drug, DOX cannot be administered in high doses due to undesirable adverse effects, mainly cardiotoxicity and thus developing a drug screening method in vitro might aid in fitting the best treatment dose and regime to the patient (Rosenblum & Peer 2014). The SNDA-DEP platform was seeded with lymphoma cells, and a low-dose gradient of DOX was generated between the wells

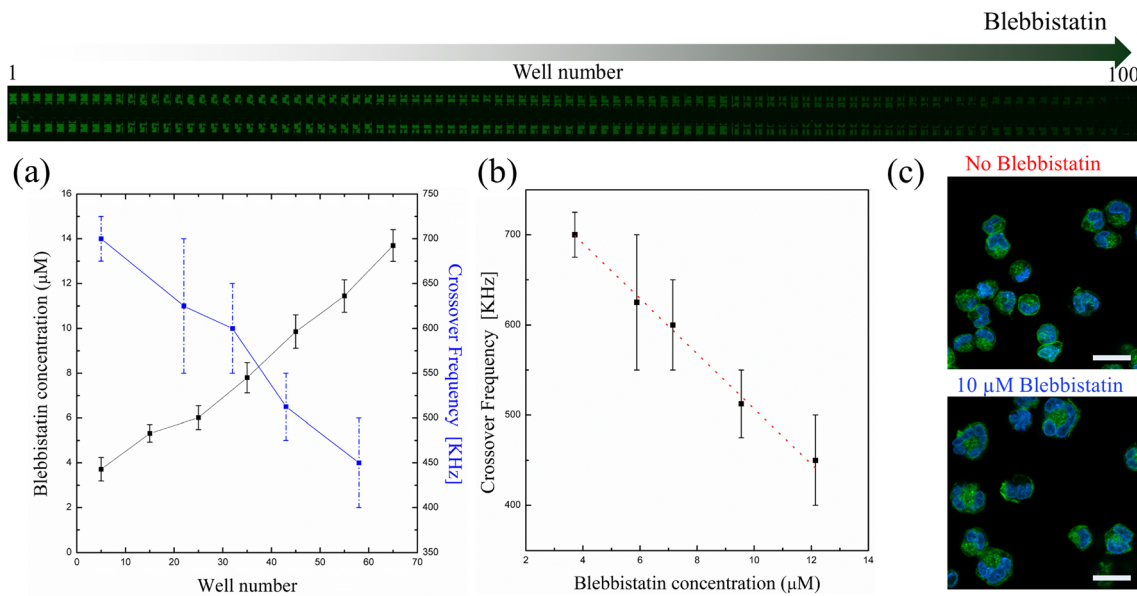


Fig. 5 Cells exposed to a blebbistatin gradient. **a** Blebbistatin concentration and cell-COF as a function of the well number inside the SNDA-DEP device after 24 h of incubation; **b** COF as a function of the blebbistatin concentration. The red dotted line indicates a linear

regression of the average COF ($R^2 = 0.994$, slope = -29.9 KHz/ μ M, intercept = 807 KHz); **c** DAPI (blue) and phalloidin (green) staining of cells after 24 h of incubation with or without blebbistatin outside the SNDA. Scale bar 20 μ m

(Markovsky et al. 2014). Figure. 6 shows the generated DOX gradient inside the platform and the cellular DEP response attributed to biological changes triggered by the DOX dose.

As the concentration of DOX increased (lower well numbers), the cell counts distinctly decreased (Fig. 6a), indicating inhibited cell proliferation. In addition, as the concentration

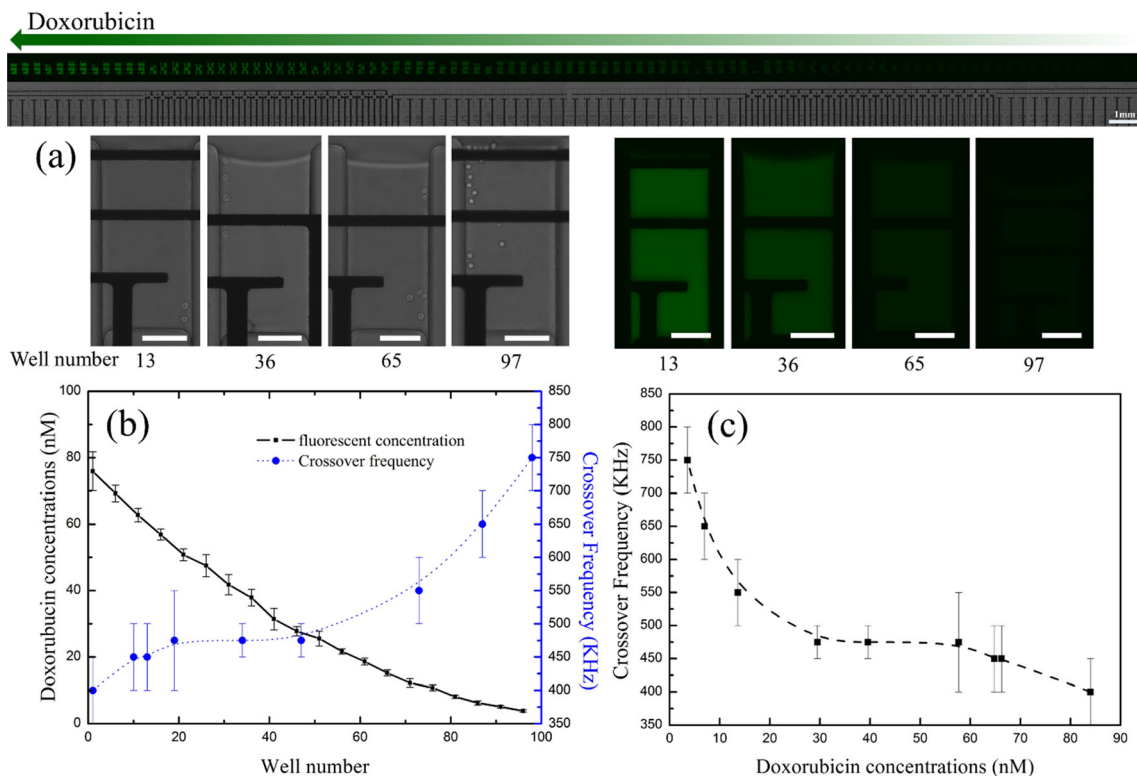


Fig. 6 Lymphoma cells exposed to a DOX gradient inside the SNDA-DEP device. **a** A depiction of the gradient formation inside the SNDA-DEP, with fluorescein as an indicator of the DOX concentration, and bright-field images of the cells; **b** Extrapolated DOX concentration and

cell COF as a function of well number inside the SNDA-DEP device, after 24 h of incubation with the drug; **c** COF as a function of the calculated DOX concentration. All scale bars are 100 μ m

of the chemotherapeutic agent increased, cell COF decreased (Fig. 6b and c).

A decrease in cell COF, from 750 to 400 KHz, was recorded as the concentration increased, but at rates that differed below and above a concentration threshold of 30 nM DOX (Fig. 6c). This non-linear dependency of the cell COF on the DOX concentration indicates saturation in the cellular response to the DOX. When cells died and underwent significant morphological changes, at DOX concentrations $>25 \mu\text{M}$, the cell COF increased dramatically and the DEP remained n-DEP, regardless of the electrodes frequency (data is not shown). According to Ye et al., DOX is responsible for morphological and cell membrane alterations and mitochondrial membrane potential collapse, which may be the underlying mechanism behind the cell COF shift (Ye et al. 2007). These results demonstrate that DEP characterization is a sensitive tool for detecting biological changes, and may be most useful in screening label-free drugs.

4 Conclusions

The SNDA-DEP microfluidic device is a reusable array of wells and electrodes that can be used to generate a controlled environment of reagents and cells of minute quantities along with individually controlled electric fields in each well. This tool enables characterization of cell behavior over a gradient of solute concentrations at the single-well resolution, using DEP. We tested the SNDA-DEP device with several experimental designs and observed that in general, lymphoma cell COF decreased with intensifying stress conditions. Moreover, a highly sensitive linear correlation between solution tonicity/blebbistatin concentration and cell COF was demonstrated. In addition DOX gradients demonstrated the capacity of the SNDA-DEP device to perform label-free drug screening assays. These results demonstrate the ability of the SNDA to characterize cell DEP in individual wells, which can be used to precisely determine the effect of solute concentration on cell response. Such a platform can be utilized as an aid for personalized medicine, for antibiotic susceptibility testing, assessment of chemotherapy and drugs doses, and to develop stem cell differentiation protocols. The SNDA-DEP device can be further extended to include additional functionalities, such as local direct conductivity measurements, electrorotation characterization as well as electroporation tests.

Acknowledgments The research was supported by MOST—Tashtiyot Grant No. 880011. The fabrication of the chip was made possible through the financial and technical support of the Technion RBNI (Russell Berrie Nanotechnology Institute) and MNFU (Micro Nano Fabrication Unit). We would like to thank Dr. Anna Scomparin and Prof. Ronit Satchi-Fainaro for the DOX sample and protocol.

References

- V.V. Abhyankar, M. A. Lokuta, A. Huttenlocher and D. J. Beebe, *Lab Chip*, 2006, 6, 389–393.
- M. Alshareef, N. Metrakos, E. Juarez Perez, F. Azer, F. Yang, X. Yang and G. Wang, *Biomicrofluidics*, 2013, 7, 11803.
- J. Avesar, T. Ben Arye and S. Levenberg, *Lab Chip*, 2014, 14, 2161–2167.
- S. Basuray and H.-C. Chang, *Phys. Rev. E Stat. Nonlinear Soft Matter Phys.*, 2007, 75, 060501.
- B.G. Chung, L. A. Flanagan, S. W. Rhee, P. H. Schwartz, A. P. Lee, E. S. Monuki and N. L. Jeon, *Lab Chip*, 2005, 5, 401–406.
- K. Cohen, R. Emmanuel, E. Kisin-Finifer, D. Shabat and D. Peer, *ACS Nano*, 2014, 8, 2183–2195.
- Y. Du, J. Shim, M. Vidula, M.J. Hancock, E. Lo, B.G. Chung, J.T. Borenstein, M. Khabiry, D.M. Cropek, A. Khademhosseini, *Lab Chip* 9, 761–767 (2009)
- M.S. Duxbury, S. W. Ashley and E. E. Whang, *Biochem. Biophys. Res. Commun.*, 2004, 313, 992–997.
- J. El-Ali, P. K. Sorger and K. F. Jensen, *Nature*, 2006, 442, 403–411.
- C. W. Frevert, G. Boggy, T. M. Keenan and A. Folch, *Lab Chip*, 2006, 6, 849–856.
- Z.R. Gagnon, *Electrophoresis*, 2011, 32, 2466–2487.
- A. Ganoth, K. C. Merimi and D. Peer, *Expert Opin. Drug Deliv.*, 2015, 12, 223–238.
- D. Gao, H. Liu, Y. Jiang, J.-M. Lin, D. Gao, H. Liu and Y. Jiang, *Trends Anal. Chem.*, 2012, 35, 150–164.
- P. Gascoyne, R. Pethig, J. Satayavivad, F. F. Becker and M. Ruchirawat, *Biochim. Biophys. Acta* 1997, 1323, 240–252.
- P.R. C. Gascoyne, J. Noshari, T. J. Anderson and F. F. Becker, *Electrophoresis*, 2009, 30, 1388–1398.
- T. Geng and C. Lu, *Lab Chip*, 2013, 13, 3803–3821.
- N.G. Green and H. Morgan, *J. Phys. Chem. B*, 1999, 103, 41–50.
- F.S. Hamdi, O. Français, E. Dufour-Gergam and B. Le Pioufle, *Bioelectrochemistry*, 2014, 100, 27–35.
- R.F. Ismagilov, A. D. Stroock, P. J. A. Kenis, G. Whitesides and H. A. Stone, *Appl. Phys. Lett.*, 2000, 76, 2376–2378.
- N.L. Jeon, S. K. W. Dertinger, D. T. Chiu, I. S. Choi, A. D. Stroock and G. M. Whitesides, *Langmuir*, 2000, 16, 8311–8316.
- K. Khoshmanesh, S. Nahavandi, S. Baratchi, A. Mitchell and K. Kalantar-zadeh, *Biosens. Bioelectron.*, 2011, 26, 1800–1814.
- D. Kim, M. A. Lokuta, A. Huttenlocher and D. J. Beebe, *Lab Chip*, 2009, 9, 1797–1800.
- S. Kim, H. J. Kim and N. L. Jeon, *Integr. Biol.*, 2010, 2, 584–603.
- J. Kolega, *Biochem. Biophys. Res. Commun.*, 2004, 320, 1020–1025.
- T. Liu, C. Li, H. Li, S. Zeng, J. Qin and B. Lin, *Electrophoresis*, 2009, 30, 4285–4291.
- E. Markovskiy, H. Baabur-Cohen and R. Satchi-Fainaro, *J. Control. Release*, 2014, 187, 145–157.
- D. Morganti and H. Morgan, *Colloids Surf. A Physicochem. Eng. Asp.*, 2011, 376, 67–71.
- B. Mosadegh, C. Huang, J.W. Park, H.S. Shin, B.G. Chung, S.-K. Hwang, K.-H. Lee, H.J. Kim, J. Brody, N.L. Jeon, *Langmuir* 23, 10910–10912 (2007)
- F.-Q. Nie, M. Yamada, J. Kobayashi, M. Yamato, A. Kikuchi and T. Okano, *Biomaterials*, 2007, 28, 4017–4022.
- S. Park, D. B. Bassat and G. Yossifon, *Biomicrofluidics*, 2014, 8, 024117.
- R. Pethig, *Biomicrofluidics*, 2010, 4, 022811.
- H.A. Pohl, H.A. Pohl, in *Dielectrophoresis: the behavior of neutral matter in nonuniform electric fields*, vol 80 (Cambridge University press, Cambridge, 1978)
- K. Ratanachoo, P. R. C. Gascoyne and M. Ruchirawat, *Biochim. Biophys. Acta* 2002, 1564, 449–458.
- D. Rosenblum and D. Peer, *Cancer Lett.*, 2014, 352, 126–136.

- L. Rozitsky, A. Fine, D. Dado, S. Nussbaum-Ben-Shaul, S. Levenberg and G. Yossifon, *Biomed. Microdevices*, 2013, 15, 859–865.
- Š. Selimović, W.Y. Sim, S.B. Kim, Y.H. Jang, W.G. Lee, M. Khabiry, H. Bae, S. Jambovane, J.W. Hong, A. Khademhosseini, *Anal. Chem.* **83**, 2020–2028 (2011)
- J. Shemesh, T.B. Arye, J. Avesar, J.H. Kang, A. Fine, M. Super, A. Meller, D.E. Ingber, S. Levenberg, *Proc. Natl. Acad. Sci.* **111**, 11293–11298 (2014)
- M. Sun, S. S. Bithi and S. A. Vanapalli, *Lab Chip*, 2011, 11, 3949–3952.
- G. Velve-Casquillas, M. Le Berre, M. Piel and P. T. Tran, *Nano Today*, 2010, 5, 28–47.
- V. Vickerman, J. Blundo, S. Chung and R. Kamm, *Lab Chip*, 2008, 8, 1468–1477.
- J. Voldman, *Annu. Rev. Biomed. Eng.*, 2006, 8, 425–454.
- S.-J. Wang, W. Saadi, F. Lin, C. Minh-Canh Nguyen and N. Li Jeon, *Exp. Cell Res.*, 2004, 300, 180–189.
- C.-G. Yang, Y.-F. Wu, Z.-R. Xu and J.-H. Wang, *Lab Chip*, 2011, 11, 3305–3312.
- N. Ye, J. Qin, X. Liu, W. Shi and B. Lin, *Electrophoresis*, 2007, 28, 1146–1153.